Construction and Building Materials 403 (2023) 133161

Contents lists available at ScienceDirect

Construction and Building Materials

journal homepage: www.elsevier.com/locate/conbuildmat

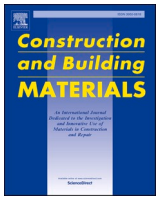

Effect of fibre diameter and tensile strength on the mechanical, fracture, and fibre distribution properties of eco-friendly high-strength self-compacting concrete

Abdullah Alshahrani [a,b], Sivakumar Kulasegaram [a,*]

[a] School of Engineering, Cardiff University, Cardiff, UK
[b] Civil Engineering Department, College of Engineering, Najran University, Najran, Saudi Arabia

ARTICLE INFO

Keywords:
Self-compacting concrete
Fibres
High Strength Concrete
Mix proportions
Eco-friendly concrete
Fibre reinforced self-compacting concrete

ABSTRACT

The development of Steel Fibre-Reinforced Self-Compacting Concrete (SFR-SCC) is a complex task with significant practical implications for the construction industry. However, the absence of established design guidelines and recommendations, and the limited availability of design methodologies, present a significant challenge. Achieving the targeted rheological and mechanical properties while simultaneously minimising production costs requires a comprehensive understanding of the optimal blend of fibre type and quantity and the coarse aggregate content. This paper addresses the impact of steel fibre properties on the rheological and fundamental mechanical properties of eco-friendly high-strength self-compacting concrete (HSSCC), using 40% ground granulated blast furnace slag (GGBS) as a cement replacement. The research focused on 30 mm long hooked-end steel fibres with tensile strengths of 1345 MPa and 3070 MPa, and diameters of 0.55 mm and 0.38 mm, respectively. In addition, the study investigated the combined effect of coarse aggregate content and steel fibre type on the performance of eco-friendly HSSCC. The fresh properties of eco-friendly HSSCC were assessed using the slump flow and J-ring tests. Furthermore, mechanical and fracture properties such as compressive strength, splitting tensile strength, elastic modulus, four-point flexural strength, and three-point flexural strength on notched prisms were also evaluated. The distribution and alignment of steel fibres in the HSSCC were assessed using image analysis techniques, which showed that the steel fibre diameters were a crucial factor in the fibre dispersion. The results demonstrated that using steel fibres with higher tensile strength and smaller diameter significantly enhanced the splitting tensile strength, flexural strength, and fracture energy, compared to steel fibres with larger diameters and lower tensile strengths. Additionally, the study indicated that the elastic modulus and fracture energy of eco-friendly HSSCC reinforced with both types of steel fibre are highly dependent on the content of coarse aggregate used. The study highlighted that the coarse aggregate proportion and the steel fibre characteristics were two vital factors that influenced the rheological and mechanical properties of HSSCC and must be considered during the mix design process to optimise the desired properties while also minimising production costs.

1. Introduction

Self-Compacting Concrete (SCC) has been one of the major construction sector developments in recent decades due to its exceptional rheological properties [1]. SCC is a highly flowable concrete that can fill every space in the formwork, preventing the formation of honeycombing without any vibration during the casting process. Due to these characteristics, the SCC becomes an excellent material for structures with intricate designs and congested reinforcement [2]. Furthermore, the reduction in the number of skilled labourers required for pouring and finishing the concrete is an important feature inherent in the use of SCC. All these advantages lead to decreased costs associated with labour and construction time compared to structures produced from conventional concrete.

However, SCC is usually designed with a high cement content, which is uneconomical and causes certain issues in concrete structures, such as hydration heat, creep, and high autogenous shrinkage [3]. Additionally, natural resource consumption and CO_2 emissions during the cement manufacturing process can have a detrimental effect on the environment [4]. These concerns can be eliminated by using mineral admixtures such

* Corresponding author.
E-mail address: kulasegarams@cardiff.ac.uk (S. Kulasegaram).

https://doi.org/10.1016/j.conbuildmat.2023.133161
Received 4 March 2023; Received in revised form 30 July 2023; Accepted 26 August 2023
Available online 4 September 2023

as GGBS, fly ash, rice ash husk, or silica fume, which are regarded as waste by-products and, as such, pose environmental risks [5]. Using GGBS as a partial cement replacement reduces the heat of hydration, improves the SCC rheological properties, and enhances durability [6]. Lee et al. [7] pointed out the significance of the proper replacement ratio of GGBS in concrete. They concluded that the optimal replacement ratio for compressive strength was 40% cement replacement and that any further GGBS addition could result in a reduction of strength. Rahla et al. [8] investigated the effects of binary-mixed concrete containing silica fume, fly ash, and GGBS at various cement replacement percentages on the functional, economic, and environmental concrete performances and found that concrete containing 40% of GGBS exhibited the highest sustainability performance level.

The use of high-strength SCC may be restricted due to its brittle behaviour, which can compromise structural integrity [9]. To improve the ductility, toughness, and flexural, shear, and tensile strengths of SCC, steel fibres may be added to form steel fibre-reinforced self-compacting concrete (SFR-SCC) [10]. However, the rheological properties of SFR-SCC are significantly impaired due to the large surface area and elongated shape of the steel fibres [11]. Therefore, the volume fraction of fibres that can be added to the SCC mix is limited and dependent on the specific mix composition and characteristics of the fibres themselves. Experimental investigations were performed on the effect of the steel fibre shapes, namely straight and hooked-end fibres, on the flexural behaviour of SCC [2]. The results demonstrated that hooked-end steel fibres performed more effectively than straight fibres in enhancing post-peak characteristics, possibly due to the improved bonding conditions provided by the deformed shape of the hooked-end fibres. Yardimci et al. [12] studied the effect of hooked-end steel fibre volume fractions, with fibre lengths of 30 mm and 60 mm, on the rheological and mechanical properties of SFR-SCC using different fine-to-coarse aggregate ratios. Results indicated that when the fibre volume fraction and length are relatively high, a higher fine-to-coarse aggregate ratio should be used to improve the flowability and fracture energy of SFR-SCC.

Şahin and Köksal demonstrated that the steel fibre tensile strength played a significant role in the flexural and splitting tensile strengths of high-strength concrete. Their results showed that using steel fibres with higher tensile strengths led to greater flexural and splitting tensile strength improvements compared to those with lower tensile strengths [13]. Additionally, a study investigated the effect of steel fibre length on the flexural behaviour of ultra-high-performance fibre-reinforced concrete (UHPFRC); the results indicated that longer steel fibres resulted in a better flexural performance but a lower fibre orientation compared to shorter fibres [14]. Alrawashdeh and Eren [15] conducted a study investigating the effect of two types of hooked-end steel fibres with aspect ratios of 60 and 80 and lengths of 30 mm and 50 mm, respectively, on the fresh, physical, and mechanical properties of SFR-SCC. The study noted the difficulties associated with mixing and placing the SCC with longer fibres (50 mm). Furthermore, the variation of the fracture parameters and brittleness of SFR-SCC with maximum aggregate size, water-to-cement ratio, and fibre content was investigated in [16]. This study's findings indicated that using a larger maximum aggregate size (19 mm) in SFR-SCC reduced the fracture energy, as it provided less space for fibre rotation.

SFR-SCC has recently become an extensively utilised material in structural and civil engineering applications such as bridges, tunnel linings, skyscrapers, slabs, and other precast concrete constructions [17]. Numerous investigations on the mechanical characteristics of fibre-reinforced concrete have been conducted [13,18]. However, only a few studies have been carried out to assess the mechanical characteristics of SFR-SCC containing high mineral admixture content [5], and minimal research was conducted to investigate the effects of fibre alignment; further study should be undertaken to analyse fibre alignment in conjunction with the aggregate content [19]. There needs to be more development in studying the effect of fibre diameter and tensile strength on the structural performance of SFR-SCC, considering the different fibre distribution degrees in the specimens. Hence an extensive experimental program has been performed to investigate the effect of fibre diameter and tensile strength on the fresh and mechanical properties of eco-friendly high-strength self-compacting concrete (HSSCC), consisting of a high GGBS content, proportioned with two coarse aggregate volume fractions as well as analysing the fibre orientation and distribution on each mix composition. SCC with steel fibres longer than 30 mm exhibited a decrease in the rheological characteristics. Thus, hooked-end steel fibres with lengths of 30 mm, diameters of 0.55 mm and 0.38 mm, and tensile strengths of 1345 and 3070 MPa, respectively, were used in this study.

2. Research significance, aim and scope

All significant aspects required for the assessment and development of eco-friendly HSSCC reinforced with two end-hooked steel fibres, with a length of 30 mm and varying in diameter and tensile strength, have been considered in this study. This HSSCC was designed with the main goal of reducing cement consumption and mitigating its environmental consequences. Accordingly, the influence of fibre diameter and tensile strength on fresh and mechanical properties of eco-friendly HSSCC designed with different coarse aggregate content was investigated. In the frame of the study, the primary performance criteria of HSSCC in the fresh properties through standard tests such as the slump flow and J-ring tests were studied, as well as the mechanical properties of hardened concrete, including compressive strength, splitting tensile strength, elastic modulus, four-point flexural strength and three-point flexural strength on notched prisms. Additionally, the fibre dispersion and orientation in HSSCC were evaluated using an image processing technique to understand the post-peak behaviour better. The results of maximum fracture energy and ductility of eco-friendly HSSCC will be obtained, with consideration of fibre type, content, and mix composition. This will allow the selection of the most efficient fibre type and content in specimens with different mix compositions. The findings of this investigation are aimed to provide the basis for choosing the proper fibre type and volume fraction for the most effective combination with coarse aggregate content. This will enable more efficient and cost-effective expenditure of steel fibre, which reduces the cost of fibre-reinforced structures and thus boosts their applicability in structural engineering.

3. Experimental programme

3.1. Materials

For cementitious materials, Portland cement (Type 1), supplied by Tarmac Cement Ltd, and ground granulated blast furnace slag (GGBS), provided by Hanson Heidelberg Cement group, were used in this study. The physical properties and chemical composition of cement and GGBS are listed in Table 1. A superplasticiser (SP), polycarboxylate ether polymer (MasterGlenium ACE 499), with a specific gravity of 1.07, was incorporated to increase the workability of the mixes. The aggregates

Table 1
Physical properties and chemical composition of cement and GGBS.

Composition	Cement	GGBS
SiO_2 (%)	19.69	34.34
Al_2O_3 (%)	4.32	12.25
Fe_2O_3 (%)	2.85	0.32
CaO (%)	63.04	39.90
MgO (%)	2.17	7.70
SO_3 (%)	3.12	0.23
Specific gravity	3.15	2.40
Fineness (m^2/kg)	384	426
Initial Setting Time (mins)	158	–
Loss on ignition (%)	3.03	0.34

consisted of crushed limestone coarse aggregate (CA) with a maximum gravel size of 10 mm and a specific gravity of 2.65, while the fine aggregate was natural river sand with a maximum particle size of 2 mm and a specific gravity of 2.55. Approximately 30% of natural river sand was replaced with a coarser fraction of limestone dust (crushed rock sand) with a specific gravity of 2.6 and particle size ranging between 2.0 mm and 0.125 mm. Such a replacement of natural river sand with a coarser fraction of limestone in concrete has the potential to save costs, be more environmentally friendly and enhance the durability of concrete [20,21]. Fig. 1 shows the fine aggregate and coarse aggregate particle size distribution curves. Dramix hooked-end steel fibres 30 mm long with diameters of 0.55 mm and 0.38 mm and tensile strengths of 1345 and 3070 MPa, respectively, were used in this study (designated as Dramix 55/30 and Dramix 80/30). The steel fibre properties are detailed in Table 2.

3.2. Mix proportion

To assess the mechanical properties and ductility of SFR-SCC, ten laboratory mix designs were prepared with 30 mm long hooked-end steel fibres with varying diameters and tensile strengths (see Table 3) to investigate the effect of steel fibre diameter and tensile strength. All mixtures were designed with a water-to-cementitious content ratio of 0.4 and 40% replacement of Portland cement by GGBS. Nevertheless, minor adjustments were made to the fine aggregate (F-A) content to account for the addition of fibre content while maintaining the w/cm ratio and CA content. Thus, these HSSCC mixes contained different volume proportions of CA, sand-to-aggregate ratios (S/A), and steel fibre volume fraction. The mixtures are designated according to their CA content, fibre diameters and steel fibre volume fractions. The control mixture is referred to as plain HSSCC and is designated according to the CA content. The mixes with hooked-end steel fibres with diameters of 0.55 mm and 0.38 mm are designated as SF55 and SF38, respectively, with the steel fibre diameters expressed in hundredths of a millimetre. The mix labels are abbreviated to feature the percentage of CA and steel fibres prominently. For instance, the mix label SF38-20–0.5 indicates an HSSCC mixture containing 0.38 mm diameter fibres, followed by the percentage of coarse aggregate and steel fibres, respectively. These HSSCC mixes were designed based on the mix design method developed by [22,23]. CA contents of 20 % and 30% were considered to evaluate the influence of CA on the properties of SFR-SCC and fibre alignment in specimens. Additionally, to assess the effects of steel fibres on the fresh and mechanical properties of eco-friendly HSSCC, steel fibre volume fractions of 0.25, 0.5, and 1% were considered.

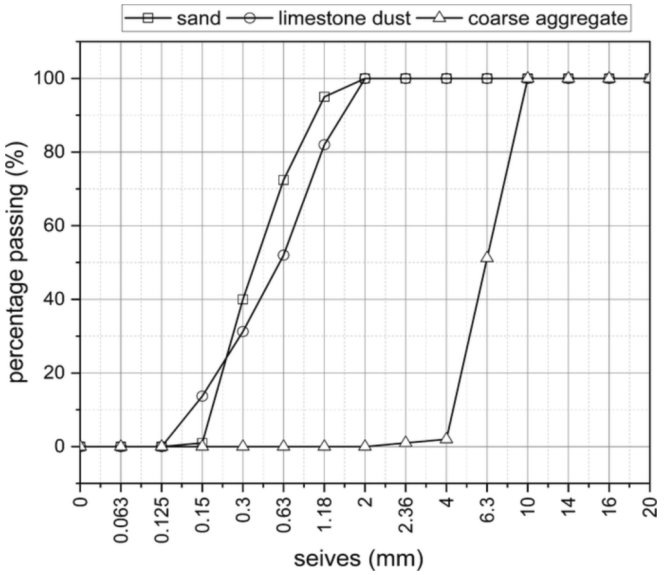

Fig. 1. Particle size distribution curves for fine and coarse aggregate.

3.3. Specimen preparation

The process of mixing the specimens was critical to achieving good dispersion of the steel fibres. The ten mixes (Table 3) were prepared in a forced action pan mixer by blending the coarsest (CA) and the finest (cement) ingredients, then the next coarsest component (fine aggregate), the next finest component (GGBS), and so on. The ingredients were mixed for approximately two minutes before each addition. Two-thirds of the SP was mixed manually with water to fluidise the dry mix, and this water-SP mixture was slowly added to the dry components and mixed for approximately four minutes. The last third of the SP was added and blended for two minutes before adding the steel fibres slowly and mixing for approximately 4 min.

It is stated in BS EN 14651 [24] and RILEM TC 162 [25] that concrete pouring should start in the centre of the mould. However, some studies suggest that pouring concrete from one end of the mould is preferred in the case of SFR-SCC [16,26]. Furthermore, Alberti et al. [27] stated that pouring in the centre can lessen the fibre dispersion in self-compacting concrete. Therefore, in this study, all moulds were poured from one end. From each mix in Table 3, eight prisms (100 mm × 100 mm × 500 mm length), eight cubes (100 mm × 100 mm × 100 mm), and six cylinders (100 mm diameter × 200 mm length) were cast. The specimens were kept under a laboratory condition for one day and then demoulded and immersed in a water tank at 20 (±1) °C for 28 days.

3.4. Test set-up and procedure

In the fresh state, the ten mixes were subjected to slump flow (flowability) and J-ring tests (passing ability) according to the recommendations in [28] and [29], respectively, to ensure that all mixes satisfied the self-compaction criteria. The cube compressive strength was determined in accordance with BS EN 12390–3 [30], while the elastic modulus (E) and the splitting tensile strength (f_{st}) were measured on cylinders as per BS EN 12390–13 [31] and BS EN 12390–6 [32], respectively. Fig. 2 depicts the experimental set-up for testing elastic modulus. The flexural strength and fracture energy were evaluated by the four-point and three-point bending tests on notched prisms. The four-point bending test was performed on four of the prisms in accordance with [33]; the experimental setup for the test is shown in Fig. 3.

The HSSCC fracture properties were measured using the three-point bending test on notched prisms, following the procedure outlined by RILEM in [34]. The mould dimensions used in this study were established in accordance with the guidelines provided in JCI-S-002–2003 [35], which specify that the side length of the prism cross-section should be at least 100 mm when the fibre length is 40 mm or less. In addition to this requirement, the mould width was designed to meet the recommendations outlined in ASTM C1609 [36], which suggest that the width (b) should be at least three times the length of the fibres being used. In the JCI standard, the notch depth (a_0) should be 0.3 times the prism depth (i.e., 30 mm), and the notch width (n_0) should not exceed 5 mm. In this experimental setup, the mid-span deflection (δ) and the crack mouth opening displacement (CMOD) of the test specimens were measured using a Linear Variable Differential Transformer (LVDT) and a clip gauge, which were attached to the knife edges on the specimens. These devices were used to record the load–deflection and load–CMOD curves of all specimens. Fig. 4 depicts the experimental setup for the three-point bending test on the notched prisms.

3.5. Determination of fracture parameter

The fracture energy is one of the most crucial factors in comprehending concrete characteristics and establishing the design criteria for large concrete structures [2,13]. The HSSCC fracture parameters were

Table 2
Properties of steel fibres.

Steel fibre code	Length l_f (mm)	Diameter, d_f (mm)	Aspect ratio (l_f/d_f)	Density (kg/m^3)	Tensile strength (MPa)	Elastic modulus (GPa)
Dramix 3D 55/30 BG	30	0.55	55	7800	1345	200
Dramix 3D 80/30 BGP	30	0.38	80	7800	3070	200

Table 3
Mix proportions of HSSCC (kg/m^3).

Mix ID	Water	Cementitious material		SP	Aggregates			Steel fibre	S/A by weight	CA	steel fibre
					F-A		CA				
		Cement	GGBS		F-A*	F-A**				By volume %	
CA-20	205.6	308.4	205.6	2.6	698.3	299.3	530	-	0.65	20	-
CA-30	205.6	308.4	205.6	2.3	517.3	221.7	796	–	0.48	30	–
SF55-20-0.25	205.6	308.4	205.6	3.0	693.8	297.3	530	19.5	0.65	20	0.25
SF55-20-0.5	205.6	308.4	205.6	3.1	689.3	295.4	530	39.0	0.65	20	0.50
SF55-20-1	205.6	308.4	205.6	3.2	680.3	291.6	530	78.0	0.65	20	1.00
SF55-30-0.5	205.6	308.4	205.6	3.0	506.3	217.0	796	39.0	0.48	30	0.50
SF38-20-0.25	205.6	308.4	205.6	3.1	693.8	297.3	530	19.5	0.65	20	0.25
SF38-20-0.5	205.6	308.4	205.6	3.4	689.3	295.4	530	39.0	0.65	20	0.50
SF38-20-1	205.6	308.4	205.6	3.6	680.3	291.6	530	78.0	0.65	20	1.00
SF38-30-0.5	205.6	308.4	205.6	3.1	506.3	217.0	796	39.0	0.48	30	0.50

F-A* refers to natural river sand; F-A** refers to a coarser fraction of limestone dust.

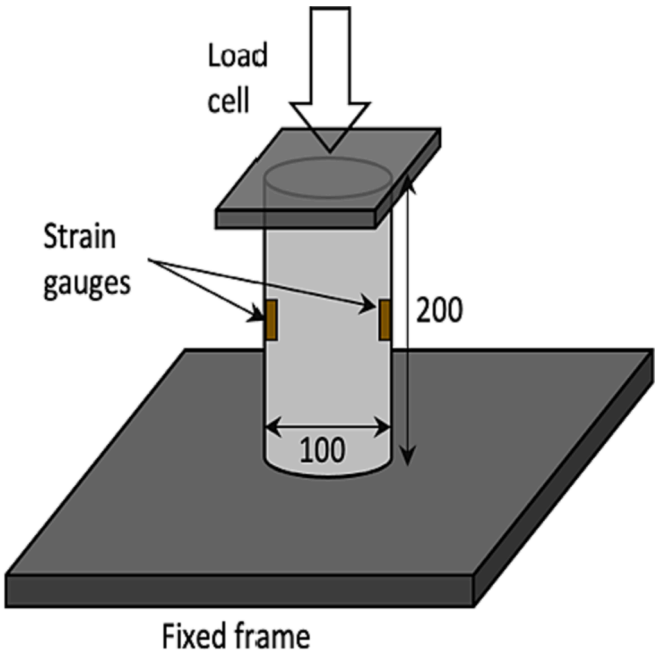

Fig. 2. Experimental setup of the elastic modulus test.

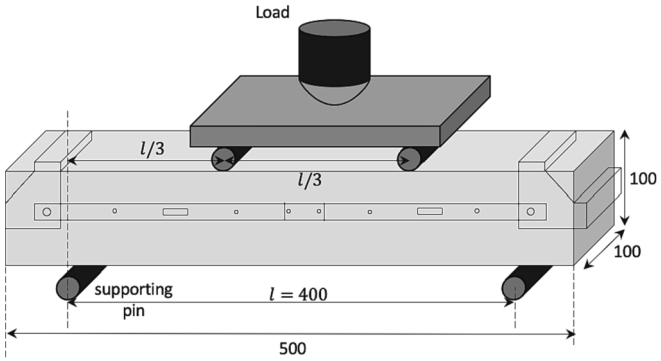

Fig. 3. Experimental setup of the four-point bending test.

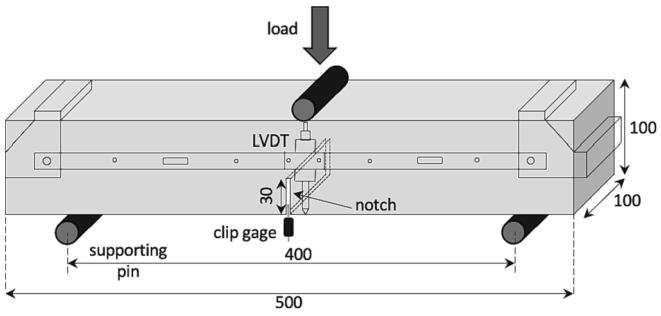

Fig. 4. Experimental setup of the three-point bending test.

determined through a three-point bending test of notched prisms, according to the RILEM recommendations [34]. The fracture energy, G_F, was determined using the equation provided by RILEM:

$$G_F = \frac{W_0 + mg\delta}{b(h - a_0)} \quad (1)$$

where W_0 is the area under the load–deflection curve (in this study, it was measured up to $\ell/150$ according to[36]), m is the specimen mass, g is the gravity, δ is the deflection at final fracture ($\ell/150$), b is the prism thickness, h is the prism depth, and a_0 is the notch depth. The energy provided by the weight of the prism itself is represented by ($mg\delta$) in the G_F equation. Hillerborg et al. [37] believed that the fracture energy of concrete alone did not provide a sufficient understanding of the concrete's brittleness or ductility and therefore proposed the characteristic length parameter to address this issue as follows:

$$L_{ch} = \frac{EG_F}{f_t^2} \quad (2)$$

where E and f_t are the elastic modulus and the tensile strength, respectively (f_{st} was used instead of f_t in this study). The characteristic length, which is proportional to the fracture energy and inversely proportional to the tensile strength, was used to assess the ductility of concrete. To produce concrete that is both strong and ductile, it is essential to achieve an appropriate balance between high fracture energy and high strength of concrete. High fracture energy contributes to the toughness of the concrete, while high strength can lead to brittleness. Ensuring that the concrete possesses both strength and ductility is crucial for its overall

performance.

Following the three-point bending test, the alignment and distribution of fibres within the cross-sections of the prism specimens were evaluated using a combination of manual inspection and image analysis. The locations at which the cross-sections were cut from the specimens are depicted in Fig. 5. The first step in this method was grinding the prism cross-sections. The cross-sectional surfaces were polished and cleaned to improve the clarity of the steel fibre sections in the cross-sections. A high-resolution camera that could capture colour (RGB) images was used to obtain clear and detailed images of the surfaces. During the image capture process, site lights were employed to enhance the visibility of the metal fibres within the cement matrix. The metal fibres had a high reflectivity level, allowing them to be easily distinguished from the cement matrix using this technique. Following the acquisition of the image, it was processed using Fiji ImageJ software to identify and distinguish steel fibres within the RGB image, a methodology employed by other researchers in the field [12,38–41]. Fig. 6(a)–(f) depicts the sequential process of analysing the cross-sectional images. It is worth noting that Fig. 6 only illustrates a small portion of a cross-section.

After conducting the image analysis, the total number of fibres intersecting the plane (N_f^T), the fibre density (d_n), the inclined angle (θ) of each fibre, and the fibre orientation factor (η_θ) can be calculated.

The fibre density (d_n) within a given area, which is the number of fibres in the unit area, can be calculated by dividing the total number of fibres detected in the cross-sections by the total area of cross-sections, as follows:

$$d_n = \frac{N_T^f}{A_c} \tag{3}$$

where N_T^f represents the total number of fibres in the cross-section, and A_c represents the area of that cross-section. The theoretical value of the density of fibres within a 3D space, denoted as d_{n3D}, can be calculated when the fibres are randomly and evenly distributed throughout the space, according to reference [41] as follows:

$$d_{n3D} = 0.5\frac{v_f}{A_f} \tag{4}$$

where v_f and A_f stand for, respectively, the fibre volume fraction in concrete and the cross-sectional area of a single fibre. The inclined angle of a single fibre (θ) to a cross-section plane can be determined as:

$$\theta = cos^{-1}\frac{d_f}{l} \tag{5}$$

where l and d_f are the length of the major axis of an elliptical fibre cross-section and the fibre diameter, respectively. The fibre orientation factor (η_θ) can be computed based on the total number of fibres at the cross-section (N_T^f) and the inclined angle as follows [38]:

$$\eta_\theta = \frac{1}{N_T^f}\sum_{i=1}^{N_T^f}\cos\theta_i \tag{6}$$

4. Results and discussion

4.1. Fresh tests

In this study, the slump flow test, which assesses the flowability of HSSCC in the absence of obstacles or hindrances, was used to evaluate the rheological properties of HSSCC mixes. The slump flow test measured the T_{500} (the time required for the concrete to flow 500 mm) and the slump flow diameter (SFD) of the fresh HSSCC mixes; the test results for the HSSCC mixes are presented in Table 4. The flow spread range was determined to be 700 ± 50 mm, and all mixes satisfied the flowability criterion without any sign of segregation or bleeding through visual inspection of fresh concrete. It is generally accepted that the incorporation of fibres into HSSCC mixtures can result in a reduction in flowability and an increase in plastic viscosity. Additionally, it is often observed that the higher the fibre aspect ratio, the greater the increase in viscosity [11]. It is important to note that the addition of steel fibres to the mix required an increased SP volume fraction to achieve the desired flowability; this effect was more pronounced in the case of fibres with a lower diameter (higher aspect ratio). Fig. 7 shows the HSSCC slump flow and J-ring test results.

The J-ring test was employed to evaluate the ability of the HSSCC mixes to pass through a configuration of reinforced bars, simulating the flow behaviour of HSSCC in real reinforced concrete structural situations. The test setup consisted of a 300 mm diameter J-ring equipped with 16 steel rods with a diameter of 16 mm for each rod. The J-ring was placed at the centre of the horizontal bottom plate, with the same circular core as the slump cone used in the slump flow test. The passing ability was evaluated by the blocking step in the J-ring test, which is a measure of the height difference between the centre and the edge of the concrete sample being tested, and the variation between flow diameter in the slump flow and the J-ring tests (Table 4). A higher blocking step suggests that the mix is more resistant to flow and has a lower passing ability, while a lower blocking step indicates that the mix is more fluid and has a better passing ability. In other words, a mix with a higher blocking step will experience greater difficulty in passing through a small opening, while a mix with a lower blocking step can flow more easily through a confined space. The J-ring test can be combined with the slump flow test to determine passing ability based on ASTM C1621/C1621M [42]. If the difference in the final spread diameter between the slump flow and J-ring flow tests is less than 25 mm, there is no visible blocking, while a difference between 25 mm and 50 mm indicates partial blockage.

In general, the incorporation of steel fibres into HSSCC mixes was found to negatively affect their passing ability, particularly in the case of fibres with a smaller diameter. This decrease in passing ability is likely due to the higher surface area and aspect ratio of the steel fibres (SF38) at a constant fibre volume content and length compared to the larger fibres (SF55). In other words, the surface area and shape of the fibres may be more effective at obstructing the flow of the HSSCC mix, leading to a decrease in its passing ability. For example, the passing ability of mix SF38-20–1 was significantly lower than that of mix SF55-20–1.

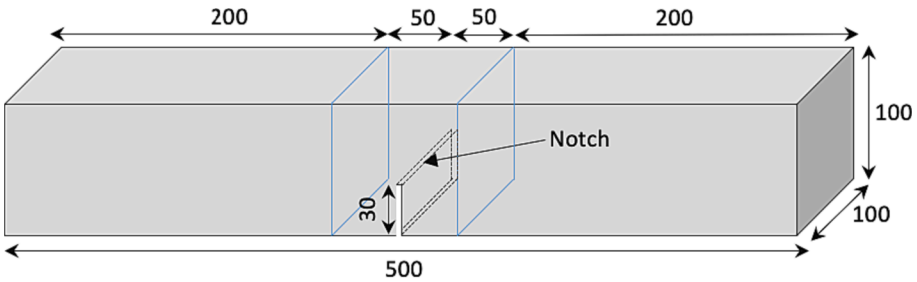

Fig. 5. Cutting locations on the prism used in the three-point bending test.

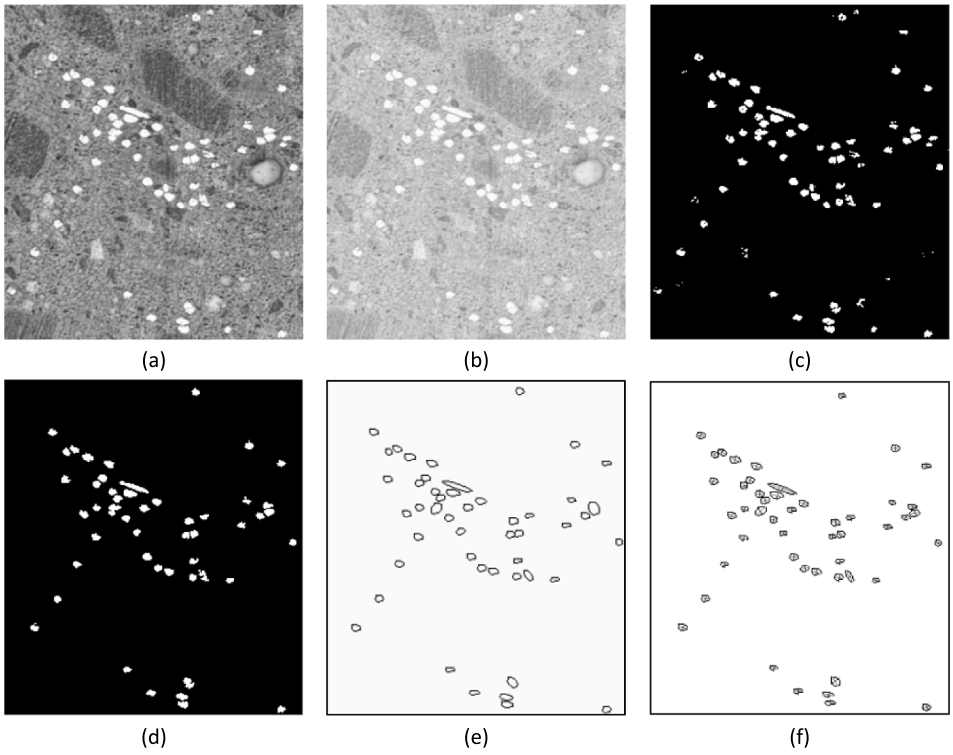

Fig. 6. Image analysis procedure: (a) RGB image, (b) grayscale image, (c) binary image using a threshold, (d) fibre identification, (e) detection of fibres borders using morphological operations, (f) calculation of θ_i based on major axes of ellipses.

Table 4
Results of slump flow and J-ring flow test of HSSCC mixes.

Mix designation	Slump flow test Spread (mm)	T_{500}(s)	J-ring flow test Spread (mm)	Blocking step (mm)	T_{500j}(s)	$D_{slump} - D_{J-ring}$
CA-20	690	1.8	670	2	2.3	20
CA-30	740	1.7	720	3	2.0	20
SF55-20-0.25	700	2.1	670	3	2.7	30
SF55-20-0.5	750	2.5	700	3	3.1	50
SF55-20-1	680	2.9	620	11	3.8	60
SF55-30-0.5	740	1.7	690	9	2.0	50
SF38-20-0.25	670	2.8	670	6	3.0	0
SF38-20-0.5	710	2.3	660	9	3.3	50
SF38-20-1	700	3.1	610	26	4.2	90
SF38-30-0.5	730	2.0	690	10	2.9	40

Other research has pointed out that the use of steel fibres with a higher length and aspect ratio can significantly reduce flowability and passing ability more than fibres with a lower length and aspect ratio [11,12,15]. Furthermore, it is widely understood that increasing the steel fibre volume fractions in SCC can increase the risk of the SCC not meeting the required passing ability standards. Yardimci et al. [12] suggested that increasing the ratio of fine to coarse aggregate (which consequently decreases the CA content) could improve the passing ability of SCC with a high steel fibre volume fraction. However, the mechanical and fracture properties of SCC can be influenced by such variations in the CA volume fraction [10]. Therefore, when adjusting the CA content to enhance the passing ability of SCC, it is important to carefully consider the potential effect on the mechanical and ductility of the HSSCC.

4.2. Mechanical performance

4.2.1. Compressive strength

It is well established that the compressive strength of HSSCC is influenced by the water-to-cementitious material ratio and the powder composition [22,43]. It has been widely recognised that the addition of steel fibres to HSSCC has an overall limited effect on the compressive strength of the composite material, but can significantly enhance its tensile, flexural, and splitting strengths and HSSCC post-peak behaviour. In the present study, the addition of steel fibres in the HSSCC led to a slight decrease in compressive strength with a reduction of approximately 1–8% for all specimens (Table 5). The study's results also indicated that the variation in the CA volume fractions and steel fibre did not significantly affect the compressive strength of HSSCC. There are conflicting reports in the literature regarding the effect of steel fibres on the compressive strength of SCC. Some studies [12,44] have shown that an increase in the percentage of hooked-end steel fibres leads to a decrease in compressive strength, while others [2,45] have found that the inclusion of hooked-end steel fibres increases compressive strength. Alrawashdeh & Eren [15] reported that the addition of fibres in an SCC mix resulted in the entrapment of additional air voids around the fibres, which had an inverse effect on the compressive strength. The effect of steel fibres on the compressive strength of HSSCC is complex and multifaceted. It has been demonstrated that the way in which steel fibres affect the rheological properties of SCC can significantly affect the compressive strength. These findings suggest that the inclusion of steel

Fig. 7. Fresh test: (a) Slump flow test, (b) J-ring test.

Table 5
Results of unit weight and compressive strength of all mixes.

Mix designation	Unit weight (kg/m^3)	Compressive strength (MPa)	
		7 days	28 days
CA-20	2322	48.4	69.5
CA-30	2398	48.2	70.4
SF55-20-0.25	2317	47.6	65.6
SF55-20-0.5	2333	46.7	66.4
SF55-20-1	2361	49.7	66.1
SF55-30-0.5	2403	47.7	69.3
SF38-20-0.25	2342	46.0	64.4
SF38-20-0.5	2344	46.1	68.2
SF38-20-1	2346	52.4	67.6
SF38-30-0.5	2418	51.6	66.7

fibres in SCC may alter the mix properties and workability of the concrete, which in turn can affect its compressive strength.

4.2.2. Elastic modulus

The measured results of the elastic modulus of HSSCC are given in Fig. 8. The findings of this study showed that the elastic modulus of HSSCC significantly increased with the addition of CA. The mix CA-30 (30% CA by volume) exhibited an elastic modulus of 41.06 GPa, while the CA-20 (20% CA by volume) mix produced an elastic modulus of 37.02 GPa, even though both mixes achieved approximately the same target compressive strength of around 70 MPa. Furthermore, the incorporation of steel fibres at a 1% volume fraction was found to enhance the elastic modulus of HSSCC by 4.13% and 3.81% for fibres with diameters of 0.55 and 0.38 mm, respectively. In contrast, the addition of 0.25% or 0.5% steel fibres, regardless of fibre characteristics, had a negligible impact on the elastic modulus of HSSCC. These results suggest that using steel fibres in HSSCC at a 1% volume fraction can improve the material's elastic modulus, while lower levels of fibre incorporation may not have a significant effect. The elastic modulus of concrete is influenced by the proportions of its individual constituents and their respective elastic moduli. As such, increasing the CA and steel fibre volume fractions in concrete can improve the concrete's elastic modulus, while an increase in the mortar content and porosity can

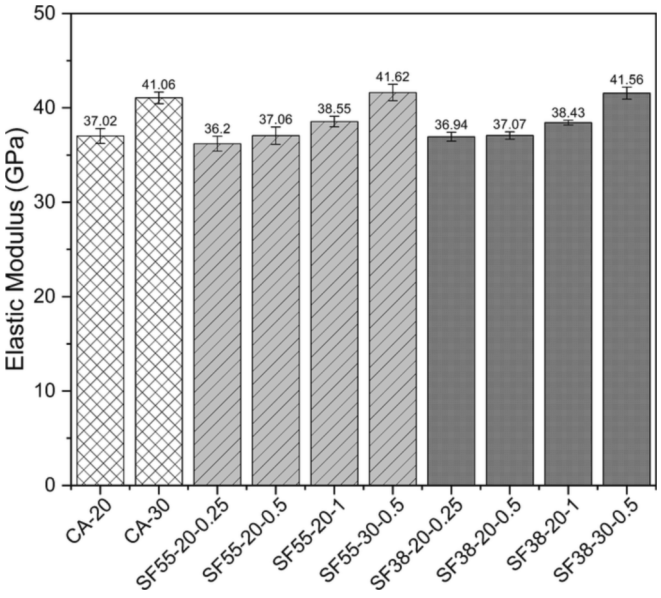

Fig. 8. Results of elastic modulus of HSSCC.

decrease the elastic modulus [10]. This correlation emphasises the importance of meticulously selecting and proportioning the various components of HSSCC to achieve the desired elastic modulus.

4.2.3. Splitting tensile strength

It was observed that the splitting tensile strength of HSSCC was significantly enhanced with an increase in the CA volume fraction and the incorporation of steel fibres with varying diameters and tensile strengths, as shown in Fig. 9. Specifically, the addition of 1% steel fibres with a diameter of 0.55 mm and lower tensile strength to HSSCC resulted in a 21.32% increase in splitting tensile strength, while the inclusion of fibres with a diameter of 0.38 mm and higher tensile strength led to a 57.97% increase in splitting tensile strength. For plain HSSCC, the difference in splitting tensile strength between mixes with varying CA content (CA-20 and CA-30) was approximately 2.79%. However, at the same volume fraction of steel fibres (0.5%), increasing the percentage of CA from 20 to 30 resulted in 9.17% and 8.3%

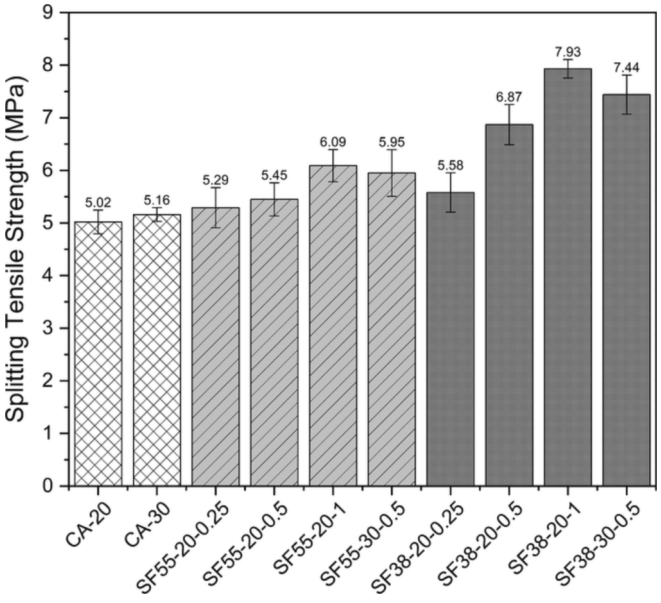

Fig. 9. Results of splitting tensile strength of HSSCC.

increased splitting tensile strength for steel fibres with diameters of 0.55 mm and 0.38 mm, respectively. This suggests that optimising the content of aggregate and fibres can improve the performance of HSSCC.

4.2.4. Flexural strength

The results of the four-point bending tests on HSSCC are presented in Fig. 10. The results showed that the flexural strength increased with the increase in CA volume fraction and the incorporation of steel fibres with different diameters and tensile strengths. Notably, the addition of steel fibres with a lower diameter and higher tensile strength significantly improved the HSSCC flexural strength. For example, at a volume fraction of 20% coarse aggregate and the incorporation of 0.25%, 5%, and 1% of steel fibres with a diameter of 0.55 mm, the flexural strength increased by 9.79%, 11.92%, and 53.03%, respectively. Similarly, at the same volume fraction of coarse aggregate and steel fibres with a diameter of 0.38 mm, the improvement was 12.10%, 43.77%, and 86.3%. Additionally, when the CA volume fraction was increased from 20% to 30% at the same steel fibre volume fraction (0.5%), the flexural strength increased by 2.07% and 7.43% for steel fibres with diameters of 0.55 mm and 0.38 mm, respectively. This suggests that optimising the content of both aggregate and fibre types can improve the performance of HSSCC. It can be seen that the mix with 0.5% of steel fibres with a diameter of 0.38 mm and 30% aggregate (SF38-30–0.5) achieved higher mechanical properties, including compressive strength, elastic modulus, splitting, and flexural strength, than the mix with 1% of steel fibres with a diameter of 0.55 mm and 20% aggregate. This demonstrates that steel fibres with a lower diameter and higher tensile strength, combined with 30% aggregate, enhance mechanical performance and can be used more efficiently and cost-effectively, reducing the cost of fibre-reinforced structures and making them more attractive for practical applications.

4.3. Fracture parameter

The influence of the CA content and the steel fibre type on the fracture energy and characteristic length of HSSCC was investigated. The results of the fracture energy and characteristic lengths of HSSCC are presented in Fig. 11 and Fig. 12. Results showed that increasing the CA content from 20% to 30% led to a 10.13% increase in fracture energy and a 14.37% increase in characteristic lengths for plain HSSCC. Fig. 13 shows the load–deflection curve of the plain HSSCC by averaging the results of four notched prisms of each mix. The results of this study regarding the influence of CA content on the HSSCC fracture parameters

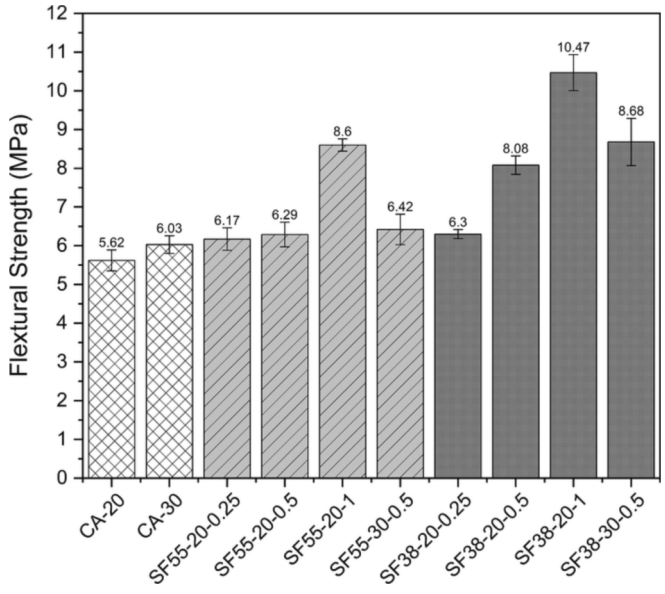

Fig. 10. Results of flexural strength obtained from four-point bending test.

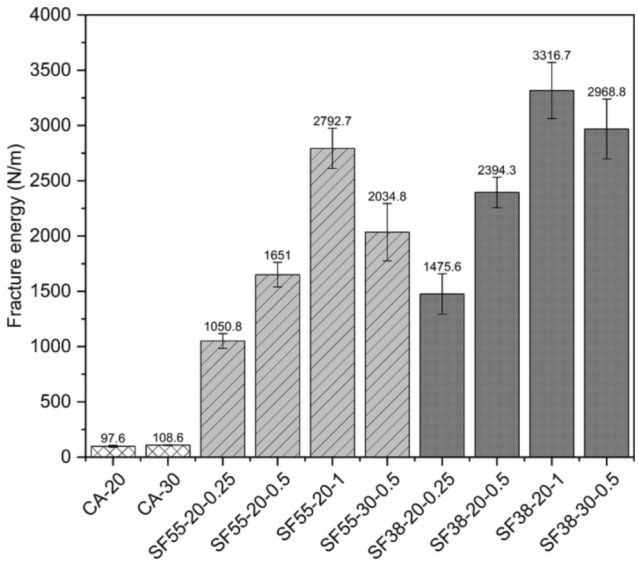

Fig. 11. Measured fracture energy from three-point bending test of HSSCC.

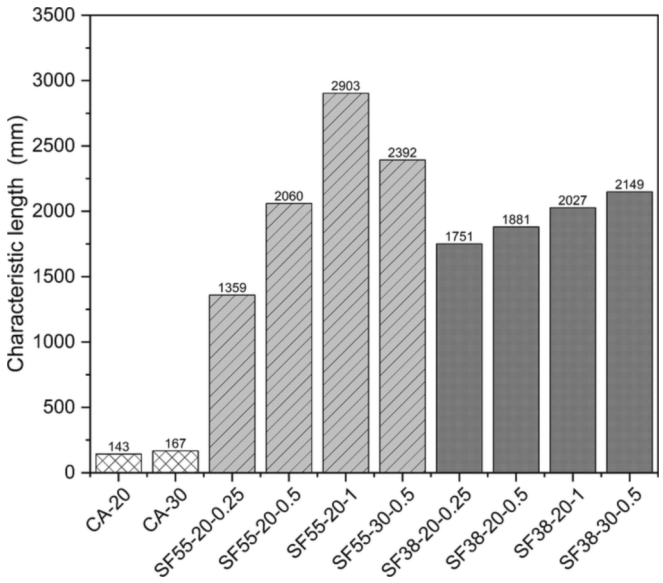

Fig. 12. Characteristic lengths of HSSCC.

are consistent with those reported by previous studies [12,46].

The addition of steel fibres to the concrete mix was found to significantly increase fracture energy, with the increase being influenced by the tensile strength and diameter of the fibres as well as the fibre content. For example, the addition of 0.25%, 0.5%, and 1% steel fibres with high tensile strength and small diameters to a concrete mix containing 20% of CA resulted in significant increases of 15.12, 24.53, and 33.98 times the fracture energy of plain concrete with 20% CA, respectively. In contrast, the inclusion of fibres with lower tensile strength and large diameter in the same mixture resulted in smaller increases in fracture energy at 10.76, 16.92, and 28.61 times, respectively. Load-deflection and load-CMOD curves, obtained from three-point bending tests on notch prisms, are plotted in Fig. 14 and Fig. 15 as a function of the steel fibre volume fraction. As can be observed, the load–deflection and load-CMOD curves of HSSCC depend on the volume fraction and the properties of the fibres. Steel fibres with high tensile strength and small diameter have a greater effect on the post-peak behaviour of HSSCC than fibres with lower tensile strength and larger diameter.

To understand the combined effects of the CA content and the steel

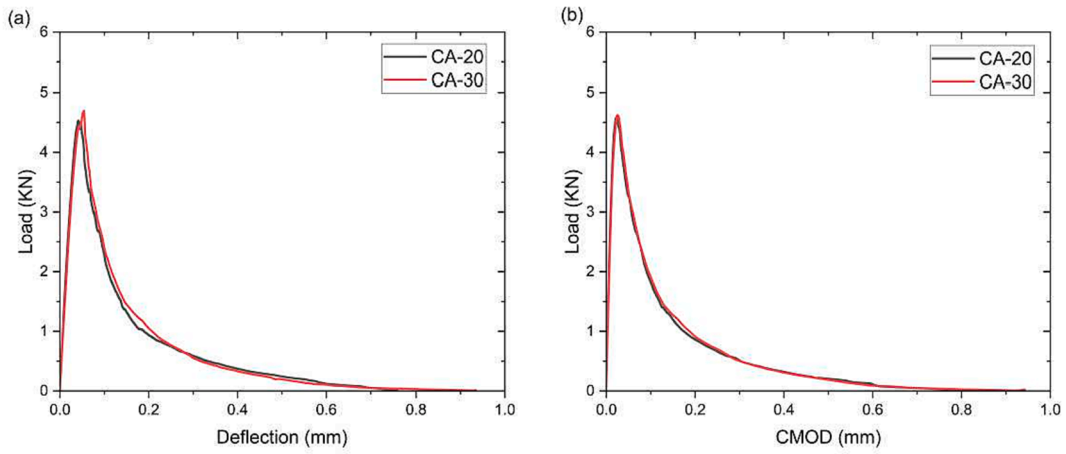

Fig. 13. The average load–deflection and Load-CMOD curves of the plain HSSCC varying by CA content.

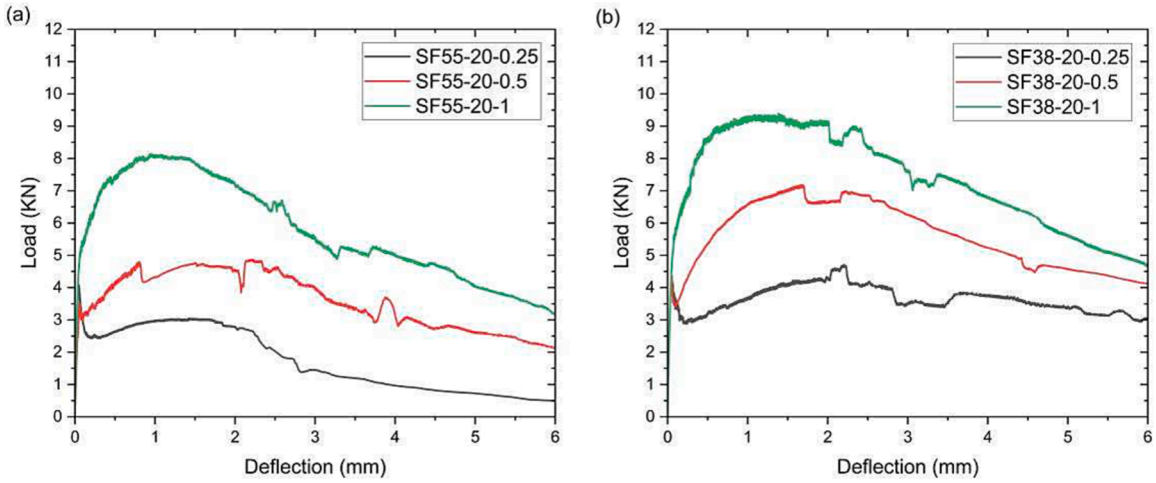

Fig. 14. Load-deflection curves of HSSCC reinforced with: (a) Dramix 55/30, (b) Dramix 80/30.

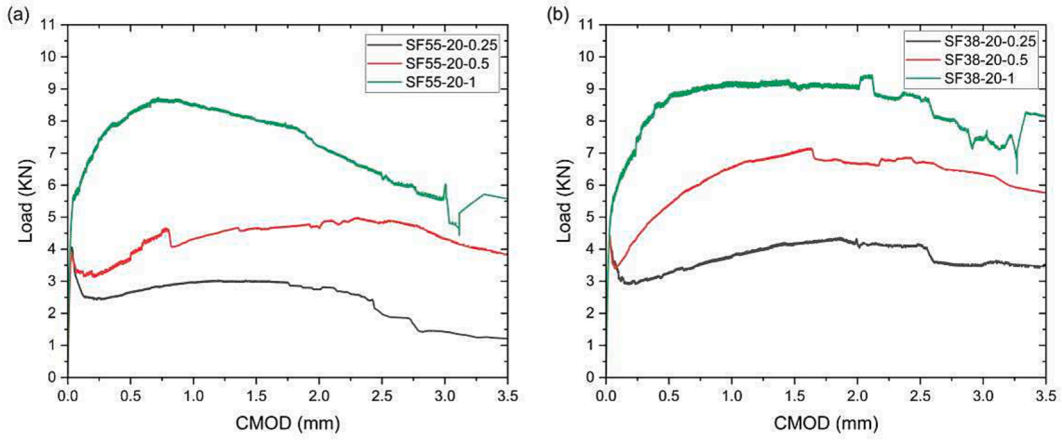

Fig. 15. Load-CMOD curves of HSSCC reinforced with: (a) Dramix 55/30, (b) Dramix 80/30.

fibre characteristics on the fracture energy of HSSCC, the CA volume fraction was increased from 20% to 30% while maintaining a constant steel fibre volume fraction (0.5%). As a result, the fracture energy increased by 23.25 % and 23.99 % for steel fibres with diameters of 0.55 mm and 0.38 mm, respectively. The load–deflection and load-CMOD curves for these combined effects are shown in Fig. 16 and Fig. 17. It can be seen that steel fibres with high tensile strength and smaller diameters have a greater positive impact on the HSSCC post-peak behaviour, regardless of the CA content. In addition, increasing the CA content at a constant steel fibre volume fraction and type significantly enhanced the HSSCC fracture properties. This observation contrasts with the findings of [12], who found that using a higher fine-to-coarse aggregate

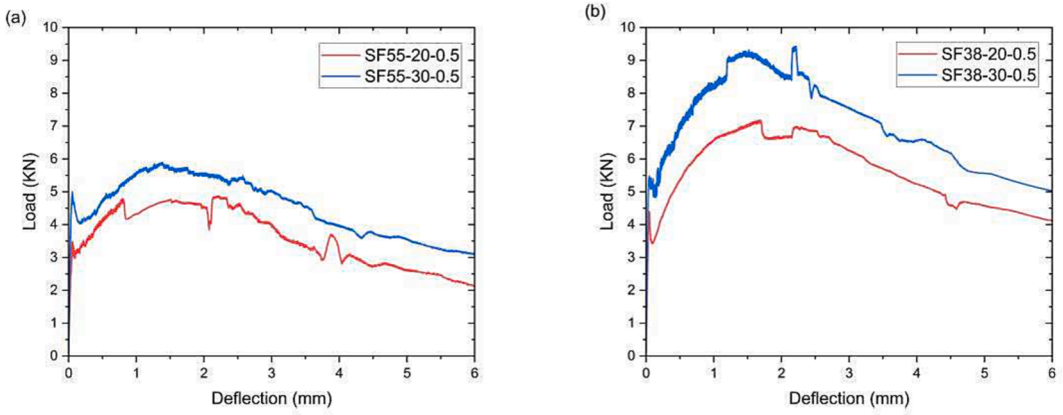

Fig. 16. Load-deflection curves of HSSCC reinforced with: (a) Dramix 55/30, (b) Dramix 80/30.

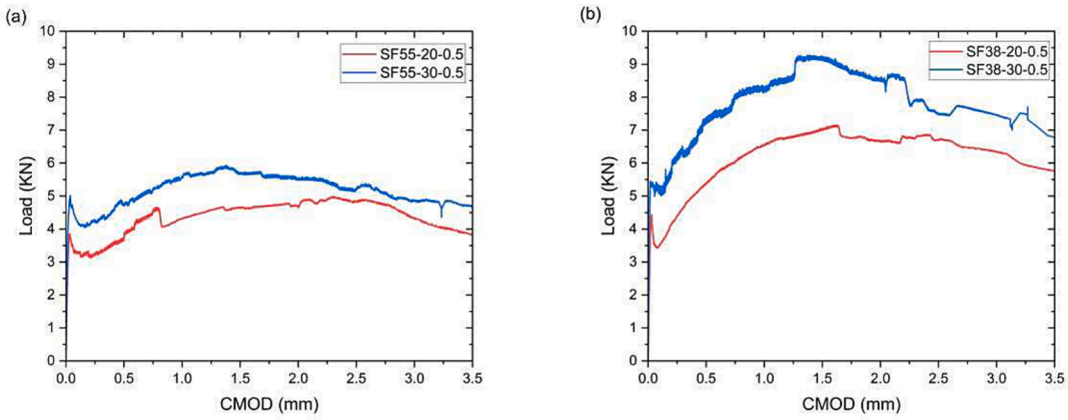

Fig. 17. Load-CMOD curves of HSSCC reinforced with: (a) Dramix 55/30, (b) Dramix 80/30.

ratio (which reduces the CA content) could improve the fracture energy of SFR-SCC when the fibre content and aspect ratio were relatively high. This discrepancy may be due to the different lengths of the steel fibres used (60 mm) and the maximum coarse aggregate size (15 mm). Ghasemi et al. [16] studied the effect of the maximum size of the coarse aggregate on different steel fibre volume fractions in SFR-SCC and found that an aggregate with a maximum size of 12.5 mm was most suitable for SFR-SCC, while using an aggregate with a maximum size of 19 mm in SFR-SCC reduced the fracture energy due to reduced space for fibre rotation. Xu et al. [47] investigated the effect of the CA content (0%, 16%, 28%, and 38%) combined with steel fibres on the mechanical properties of high-performance concrete (HPC) and found that the optimal level of coarse aggregate in HPC was approximately 28%.

The design of mix compositions for SFR-SCC is a challenging area of research and development in the construction industry [10]. It requires a thorough understanding of the optimal combinations of steel fibre type and content as well as CA content to achieve the desired rheological and mechanical concrete properties while maintaining economical production costs. The experimental investigation has shown that a mix composition with 0.5% steel fibres of 0.38 mm diameter and 30% of CA (SF38-30–0.5) performs better in terms of fracture energy than a mix with 1% steel fibres of 0.55 mm diameter and 20% aggregate (SF55-20–1). This indicates that steel fibres with a lower diameter and higher tensile strength, in combination with a higher aggregate content (30%), are more effective at increasing fracture energy and can be used more efficiently and cost-effectively, potentially reducing the cost of fibre-reinforced structures and making them more viable for practical applications. The CA content and the fibre properties are two important factors contributing to the performance of SFR-SCC and should be considered carefully in the mix design process.

4.4. Evaluation of fibre distribution

The use of steel fibres in concrete can significantly improve its post-peak load-bearing capacity, with the extent of improvement depending on the type, volume fraction, and orientation of the fibres. There is a strong relationship between the number of fibres on the fracture surfaces and the composite's post-peak behaviour [48]. Table 6 presents various fibre distribution characteristics, including fibre density, theoretical fibre density, and the fibre orientation factor. The results demonstrate that increasing the fibre volume fraction, regardless of the type of steel fibres used, leads to a corresponding increase in fibre density. However, it can be observed that the fibre density was significantly higher with fibres of smaller diameter (0.38 mm) compared to fibres of larger diameter (0.55 mm) at the same volume fraction. For example, the fibre density of the mix SF55-20–0.25 was 0.64 fibres/cm^2, while in the mix SF38-20–0.25, it was almost double at 1.34 fibres/cm^2. Yoo et al. [14] showed that fibre density was not significantly affected by the fibre length when fibres were used with different aspect ratios but the same diameters. This study suggests that fibre diameter plays a significant role in the number of fibres on the fracture surfaces of HSSCC.

In addition, the measured fibre density (d_n) was higher than the theoretical fibre density (d_{n3D}) across all mixes HSSCC. This difference in density can be attributed to the high flowability of the HSSCC and the influence of the wall effect [41,49]. The fibre orientation factor generally increased with the increase in the content of both types of steel fibres. The fibre orientation factor had a range of 0.68–0.78 and 0.67–0.77 for fibres with diameters of 0.55 mm and 0.38 mm,

Table 6
Results of fibre density d_n, theoretical fibre density d_{n3D}, and the fibre orientation factor..η_θ

	SF55-20-0.25	SF55-20-0.5	SF55-20-1	SF55-30-0.5	SF38-20-0.25	SF38-20-0.5	SF38-20-1	SF38-30-0.5
d_n	0.64	1.41	2.56	1.44	1.34	2.71	5.22	2.40
d_{n3D}	0.53	1.05	2.10	1.05	1.10	2.20	4.41	2.20
η_θ	0.68	0.74	0.74	0.78	0.67	0.74	0.77	0.74

respectively. When the CA content in HSSCC with steel fibres was increased from 20% to 30%, the fibre orientation factor increased from 0.74 to 0.78 for fibres with a diameter of 0.55 mm. However, for fibres with a diameter of 0.38 mm, there was no significant change in the fibre orientation factor with increased aggregate content. Further studies are necessary to analyse the influence of varying sizes and proportions of CA and steel fibre dimensions on the three-dimensional distribution of steel fibres in HSSCC. Further investigations in this area will facilitate the advancement of knowledge regarding the influence of CA and the geometry of steel fibres on the efficacy of short steel fibre reinforcement in HSSCC. This study will have implications for the optimisation of reinforcement strategies in HSSCC.

5. Conclusions

Designing the composition of steel fibre-reinforced self-compacting concrete (SFR-SCC) is a complex task in the construction industry, as it requires a detailed understanding of the optimal combination of fibre type and content, as well as the amount of coarse aggregate to achieve the desired rheological and mechanical properties while also minimising production costs. This study investigated the performance of eco-friendly HSSCC, made of cement and GGBS, reinforced with end-hooked steel fibres of different diameters and tensile strengths. The results showed that the inclusion of both types of steel fibres in the HSSCC significantly improved its flexural and splitting strengths, as well as its post-peak behaviour, while only slightly reducing its compressive strength. Additionally, the use of steel fibres with higher tensile strength and smaller diameter resulted in greater improvement in splitting tensile strength, flexural strength and fracture energy compared to fibres with a larger diameter and lower tensile strength. The study also indicates that the diameter of the steel fibres is a crucial factor in the dispersion of steel fibres within HSSCC. The findings suggest that steel fibres with a lower diameter and higher tensile strength, along with a higher content of coarse aggregate, are more effective at increasing the mechanical and fracture properties and can be used more efficiently and cost-effectively, potentially reducing the cost of fibre-reinforced structures and making them more feasible for practical use. The elastic modulus and post-peak behaviour of HSSCC reinforced with both types of steel fibres are significantly influenced by changes in coarse aggregate content. The content of coarse aggregate and the properties of the fibres are two critical factors that impact the performance of SFR-SCC and should be carefully considered in the mix design process.

CRediT authorship contribution statement

Abdullah Alshahrani: Conceptualization, Methodology, Writing – original draft. **Sivakumar Kulasegaram:** Project administration, Supervision, Writing – review & editing.

Declaration of Competing Interest

The authors declare that they have no known competing financial interests or personal relationships that could have appeared to influence the work reported in this paper.

Data availability

Data will be made available on request.

References

[1] P. Dinakar, S.N. Manu, Concrete mix design for high strength self-compacting concrete using metakaolin, Mater. Des. 60 (2014) 661–668, https://doi.org/10.1016/j.matdes.2014.03.053.
[2] M. Pająk, T. Ponikiewski, Flexural behavior of self-compacting concrete reinforced with different types of steel fibers, Constr. Build. Mater. 47 (2013) 397–408.
[3] M. Jalal, A. Pouladkhan, O.F. Harandi, D. Jafari, Comparative study on effects of Class F fly ash, nano silica and silica fume on properties of high performance self compacting concrete, Constr. Build. Mater. 94 (2015) 90–104, https://doi.org/10.1016/j.conbuildmat.2015.07.001.
[4] A. Adesina, P. Awoyera, Overview of trends in the application of waste materials in self-compacting concrete production, SN Appl Sci. 1 (2019) 1–18, https://doi.org/10.1007/s42452-019-1012-4.
[5] V. Athiyamaan, G. Mohan Ganesh, Experimental, statistical and simulation analysis on impact of micro steel – Fibres in reinforced SCC containing admixtures, Constr. Build. Mater. 246 (2020) 118450.
[6] O. Boukendakdji, E.H. Kadri, S. Kenai, Effects of granulated blast furnace slag and superplasticizer type on the fresh properties and compressive strength of self-compacting concrete, Cem. Concr. Compos. 34 (2012) 583–590, https://doi.org/10.1016/j.cemconcomp.2011.08.013.
[7] H.S. Lee, X.Y. Wang, L.N. Zhang, K.T. Koh, Analysis of the optimum usage of slag for the compressive strength of concrete, Materials. 8 (2015) 1213–1229, https://doi.org/10.3390/ma8031213.
[8] K.M. Rahla, R. Mateus, L. Bragança, Comparative sustainability assessment of binary blended concretes using Supplementary Cementitious Materials (SCMs) and Ordinary Portland Cement (OPC), J. Clean. Prod. 220 (2019) 445–459, https://doi.org/10.1016/j.jclepro.2019.02.010.
[9] R. Deeb, B.L. Karihaloo, S. Kulasegaram, Reorientation of short steel fibres during the flow of self-compacting concrete mix and determination of the fibre orientation factor, Cem. Concr. Res. 56 (2014) 112–120, https://doi.org/10.1016/j.cemconres.2013.10.002.
[10] A. Alshahrani, S. Kulasegaram, A. Kundu, Elastic modulus of self-compacting fibre reinforced concrete: Experimental approach and multi-scale simulation, Case Stud. Constr. Mater. 18 (2023) e01723.
[11] R. Deeb, A. Ghanbari, B.L. Karihaloo, Development of self-compacting high and ultra high performance concretes with and without steel fibres, Cem. Concr. Compos. 34 (2012) 185–190, https://doi.org/10.1016/j.cemconcomp.2011.11.001.
[12] M.Y. Yardimci, B. Baradan, M.A. Taşdemir, Effect of fine to coarse aggregate ratio on the rheology and fracture energy of steel fibre reinforced self-compacting concretes, Sadhana 39 (2014) 1447–1469, https://doi.org/10.1007/s12046-014-0257-2.
[13] Y. Şahin, F. Köksal, The influences of matrix and steel fibre tensile strengths on the fracture energy of high-strength concrete, Constr. Build. Mater. 25 (2011) 1801–1806, https://doi.org/10.1016/j.conbuildmat.2010.11.084.
[14] D.Y. Yoo, N. Banthia, Y.S. Yoon, Predicting the flexural behavior of ultra-high-performance fiber-reinforced concrete, Cem. Concr. Compos. 74 (2016) 71–87, https://doi.org/10.1016/j.cemconcomp.2016.09.005.
[15] A. Alrawashdeh, O. Eren, Mechanical and physical characterisation of steel fibre reinforced self-compacting concrete: Different aspect ratios and volume fractions of fibres, Resul. Eng. 13 (2022), 100335, https://doi.org/10.1016/j.rineng.2022.100335.
[16] M. Ghasemi, M.R. Ghasemi, S.R. Mousavi, Studying the fracture parameters and size effect of steel fiber-reinforced self-compacting concrete, Constr. Build. Mater. 201 (2019) 447–460, https://doi.org/10.1016/j.conbuildmat.2018.12.172.
[17] C. Bao, J.H. Bi, D. Xu, J. Guan, W.X. Cheng, Numerical simulation of the distribution and orientation of steel fibres in SCC, Mag. Concr. Res. 72 (2020) 1102–1111, https://doi.org/10.1680/jmacr.18.00432.
[18] M.T. Kazemi, H. Golsorkhtabar, M.H.A. Beygi, M. Gholamitabar, Fracture properties of steel fiber reinforced high strength concrete using work of fracture and size effect methods, Constr. Build. Mater. 142 (2017) 482–489, https://doi.org/10.1016/j.conbuildmat.2017.03.089.
[19] H. Huang, X. Gao, L. Teng, Fiber alignment and its effect on mechanical properties of UHPC: An overview, Constr. Build. Mater. 296 (2021), 123741, https://doi.org/10.1016/j.conbuildmat.2021.123741.
[20] K. S.k., S.K. Singh, A. Chourasia, Alternative fine aggregates in production of sustainable concrete- A review, J. Clean. Prod. 268 (2020) 122089.
[21] M.S. Abo Dhaheer, M.M. Al-Rubaye, W.S. Alyhya, B.L. Karihaloo, S. Kulasegaram, Proportioning of self-compacting concrete mixes based on target plastic viscosity and compressive strength: Part II - experimental validation, J. Sustain Cem. Based Mater. 5 (2016) 217–232, https://doi.org/10.1080/21650373.2015.1036952.
[22] M.S. Abo Dhaheer, M.M. Al-Rubaye, W.S. Alyhya, B.L. Karihaloo, S. Kulasegaram, Proportioning of self–compacting concrete mixes based on target plastic viscosity and compressive strength: Part I - mix design procedure, J. Sustain Cem. Based Mater. 5 (2016) 199–216, https://doi.org/10.1080/21650373.2015.1039625.

[23] R. Deeb, B.L. Karihaloo, Mix proportioning of self-compacting normal and high-strength concretes, Mag. Concr. Res. 65 (2013) 546–556, https://doi.org/10.1680/macr.12.00164.
[24] BS EN 14651, Test Method for Metallic Fibre Concrete. Measuring the Flexural Tensile Strength (Limit of Proportionality (LOP), Residual), (2007).
[25] Rilem TC 162-TDF, Rilem TC 162-TDF: Test and design methods for steel fibre reinforced concrete - Bending test (Final Recommendation), Materials and Structures/Materiaux et Constructions. 35 (2002) 579–582. https://doi.org/10.1617/13884.
[26] S. Grunewald, Performance-based design of self-compacting fibre reinforced concrete, Delft University Press,Delft (The Netherlands), 2004. http://repository.tudelft.nl/view/ir/uuid:07a817aa-cba1-4c93-bbed-40a5645cf0f1/.
[27] M.G. Alberti, A. Enfedaque, J.C. Gálvez, Fracture mechanics of polyolefin fibre reinforced concrete: Study of the influence of the concrete properties, casting procedures, the fibre length and specimen size, Eng. Fract. Mech. 154 (2016) 225–244, https://doi.org/10.1016/j.engfracmech.2015.12.032.
[28] BS EN 12350-8, 12350-8 Testing fresh concrete, Self-Compacting Concrete. Slump-Flow Test. (2010) 18.
[29] BS EN 12350-12, 12350-12 Testing fresh concrete, Self-Compacting Concrete. J-Ring Test. (2010) 18.
[30] BS EN 12390-3, Testing hardened concrete: compressive strength of test specimens, (2009).
[31] BS EN 12390-13, Determination of secant modulus of elasticity in compression, (2019).
[32] BS EN 12390-6, Testing hardened concrete — Part 6: Tensile splitting strength of test specimens, British Standard. (2000).
[33] BS EN 12390-5, Testing hardened concrete Part 5: Flexural strength of test specimens, British Standard. 38 (2009) 195–217.
[34] RILEM Fmc-50,, Determination of the fracture energy of mortar and concrete by means of three-point bend tests on notched beams, Mater. Struct. 18 (1985) 285–290.
[35] JCI-S-002-2003, Method of Test for Load-Displacement Curve of Fiber Reinforced Concrete by Use of Notched Beam, Japan Concrete Institute Standard Method. (2003) 1–6.
[36] ASTM C1609, Standard Test Method for Flexural Performance of Fiber Reinforced Concrete (Using Beam with Third-point Loading), (2007) 1–8.
[37] A. Hillerborg, M. Modéer, P.-E. Petersson, Analysis of crack formation and crack growth in concrete by means of fracture mechanics and finite elements, Cem Concr. Res. 6 (6) (1976) 773–781.
[38] A. Abrishambaf, J.A.O. Barros, V.M.C.F. Cunha, Relation between fibre distribution and post-cracking behaviour in steel fibre reinforced self-compacting concrete panels, Cem. Concr. Res. 51 (2013) 57–66, https://doi.org/10.1016/j.cemconres.2013.04.009.
[39] H. Huang, X. Gao, L. Li, H. Wang, Improvement effect of steel fiber orientation control on mechanical performance of UHPC, Constr. Build. Mater. 188 (2018) 709–721, https://doi.org/10.1016/j.conbuildmat.2018.08.146.
[40] Y. Zhao, J. Bi, Z. Wang, L. Huo, J. Guan, Y. Zhao, Y. Sun, Numerical simulation of the casting process of steel fiber reinforced self-compacting concrete: Influence of material and casting parameters on fiber orientation and distribution, Constr. Build. Mater. 312 (2021), 125337, https://doi.org/10.1016/j.conbuildmat.2021.125337.
[41] Y. Zhao, J. Bi, L. Huo, Z. Wang, J. Guan, Y. Zhao, Development of a coupled numerical framework of steel fiber reinforced self-compacting concrete, Constr. Build. Mater. 303 (2021), 124582, https://doi.org/10.1016/j.conbuildmat.2021.124582.
[42] ASTM C1621, Standard Test Method for Passing Ability of Self-Consolidating Concrete by J-Ring, (2014).
[43] A. Alshahrani, T. Cui, S. Kulasegaram, Effect of Sand to Aggregate Ratio on the Properties of Self-Compacting High-Performance Concrete, Int. J. Civil Infrastruct. 5 (2022). https://doi.org/10.11159/ijci.2022.006.
[44] A. Khaloo, E.M. Raisi, P. Hosseini, H. Tahsiri, Mechanical performance of self-compacting concrete reinforced with steel fibers, Constr. Build. Mater. 51 (2014) 179–186, https://doi.org/10.1016/j.conbuildmat.2013.10.054.
[45] P.A. Sivanantham, G.G. Prabhu, G.G. Vimal Arokiaraj, K. Sunil, S.J.S. Chelladurai, Effect of Fibre Aspect-Ratio on the Fresh and Strength Properties of Steel Fibre Reinforced Self-Compacting Concrete, Adv. Mater. Sci. Eng. 2022 (2022) 1–8.
[46] W.S. Alyhya, M.S. Abo Dhaheer, M.M. Al-Rubaye, B.L. Karihaloo, Influence of mix composition and strength on the fracture properties of self-compacting concrete, Constr. Build. Mater. 110 (2016) 312–322, https://doi.org/10.1016/j.conbuildmat.2016.02.037.
[47] L. Xu, F. Wu, Y. Chi, P. Cheng, Y. Zeng, Q. Chen, Effects of coarse aggregate and steel fibre contents on mechanical properties of high performance concrete, Constr. Build. Mater. 206 (2019) 97–110, https://doi.org/10.1016/j.conbuildmat.2019.01.190.
[48] R. Zerbino, J.M. Tobes, M.E. Bossio, G. Giaccio, On the orientation of fibres in structural members fabricated with self compacting fibre reinforced concrete, Cem. Concr. Compos. 34 (2012) 191–200, https://doi.org/10.1016/j.cemconcomp.2011.09.005.
[49] R.A. Raju, S. Lim, M. Akiyama, T. Kageyama, Effects of concrete flow on the distribution and orientation of fibers and flexural behavior of steel fiber-reinforced self-compacting concrete beams, Constr. Build. Mater. 262 (2020), 119963, https://doi.org/10.1016/j.conbuildmat.2020.119963.